

Article

# Effect of Functionalization with Potassium Atoms on the Electronic Properties of a 3D Glass-like Nanomaterial Reinforced with Carbon Nanotubes: In Silico Study

Alexander A. Petrunin <sup>1</sup>, Michael M. Slepchenkov <sup>1</sup> and Olga E. Glukhova <sup>1,2,\*</sup>

<sup>1</sup> Institute of Physics, Saratov State University, Astrakhanskaya Street 83, 410012 Saratov, Russia; sacha.petrynin@gmail.com (A.A.P.); slepchenkovm@mail.ru (M.M.S.)

<sup>2</sup> Laboratory of Wearable Biocompatible Devices and Bionic Prostheses, I.M. Sechenov First Moscow State Medical University, Trubetskaya Street 8-2, 119991 Moscow, Russia

\* Correspondence: glukhova@info.sgu.ru; Tel.: +7-8452-514562

**Abstract:** In this paper, using the self-consistent charge density-functional tight-binding (SCC DFTB) method, we perform an in silico study of the effect of functionalization by potassium atoms on the electronic properties of a new configuration of the glass-like carbon (GLC) reinforced with (4,4) and (6,5) single-walled carbon nanotubes (SWCNTs). The method of classical molecular dynamics was used to obtain energetically stable GLC configurations with different mass fractions of potassium. It is found that with an increase in the mass fraction of SWCNTs, the elasticity of GLC increases. It is shown that when the GLC structure reinforced with SWCNTs is filled with potassium, the number of available electronic states at the Fermi level increases compared to GLC without nanotubes, which significantly improves the emission and electrophysical characteristics of the carbon nanomaterial. For most structures, at a potassium/carbon mass ratio of 1:100 (0.01), an increase in the Fermi energy is observed, and, hence, a decrease in the work function. The maximum decrease in the work function by ~0.3 eV was achieved at a mass ratio of potassium/carbon of 1:4.5 (0.23) for GLC reinforced with (6,5) SWCNTs. It is revealed that, at a mass ratio of potassium/carbon of 1:28.5 (0.035), the quantum capacitance of GLC reinforced with (4,4) and (6,5) SWCNTs increases by ~9.4% (1752.63 F/g) and 24.1% (2092.04 F/g), respectively, as compared to GLC without nanotubes (1587.93 F/g). Based on the results obtained, the prospects for the application of the proposed GLC configuration in emission electronics devices are predicted.

**Keywords:** glass-like carbon; single-walled carbon nanotubes; SCC DFTB method; density of states; Fermi energy; quantum capacitance; work function; molecular dynamics



**Citation:** Petrunin, A.A.; Slepchenkov, M.M.; Glukhova, O.E. Effect of Functionalization with Potassium Atoms on the Electronic Properties of a 3D Glass-like Nanomaterial Reinforced with Carbon Nanotubes: In Silico Study. *J. Compos. Sci.* **2022**, *6*, 186. <https://doi.org/10.3390/jcs6070186>

Academic Editors: Ilaria Armentano and Marco Monti

Received: 1 June 2022

Accepted: 21 June 2022

Published: 24 June 2022

**Publisher's Note:** MDPI stays neutral with regard to jurisdictional claims in published maps and institutional affiliations.



**Copyright:** © 2022 by the authors. Licensee MDPI, Basel, Switzerland. This article is an open access article distributed under the terms and conditions of the Creative Commons Attribution (CC BY) license (<https://creativecommons.org/licenses/by/4.0/>).

## 1. Introduction

Due to their promising properties, GLC nanomaterials are in demand and very relevant in a wide range of applications [1–15]. These materials have high thermal stability, mechanical strength, abrasion resistance, and chemical inertness, as well as isotropic electrical conductivity [2–4,15–17]. They are characterized by the presence of a large number of nanopores; that is, their density has clearly defined local regions with a high density several times higher than the average value. That is, the atomic structure is also characterized by islands of increased density formed by the accumulation of fragments of graphene flakes, nanotubes, and fullerene caps in separate local places. Modern technology allows us to control the size of nanopores. For example, when forming GLC on a conductive substrate, the nanopore size can be varied from 0.6 to 4.0 nm. The samples of such nanoporous GLC were fabricated as a result of the thermochemical treatment of different carbides with chlorine at different temperatures [18,19]. The modern capabilities of computer modeling allow one to study all the features of carbon surface modification at the atomic level [20]. In

most studies, the GLC structure is represented mainly by graphene flakes (mono-/bi-layer), layered graphene, and fullerene fragments [21–24].

GLC nanomaterials are promising materials for the manufacture of lithium-ion batteries [6,7] and capacitors [8] due to their anomalously high capacitance [9], as well as for creating on the basis of sensors for the detection of dopamine [10], adrenaline [11], chlorpromazine [12], and methyl dopa [13]. Carbon nanoporous glass-like materials are also actively used in modern emission electronics [1,25–28], in particular, for the fabrication of field cathodes based on them. Such cathodes have promising field emission parameters. The edges of the pores in these carbon glass-like materials are sharp, blade-like structures that make them centers of radiation. The increasing interest in the GLC nanomaterial in recent times is due to increasing possibilities of modifying its pores with atoms of various chemical elements [29–31]. Thus, it was shown that when GLC is doped with potassium atoms, it is possible to reduce the work function of electrons due to the redistribution of electron density on GLC atoms [4]. Difficulties in the implementation of this process may arise due to the disordered atomic structure of GLC, which is a mixture of various carbon nanoobjects. A possible solution to this problem could be the use of carbon nanotubes as reinforcing inclusions of GLC nanomaterial. As is known, the mass fraction of these carbon nanostructures is controlled by temperature during the synthesis [24].

In this paper, we consider the possibility of controlling the electrophysical properties and characteristics of GLC reinforced with SWCNTs via functionalization with potassium atoms. According to our assumption, the high elasticity of nanotubes will allow more potassium to be stored in the pores of GLC as compared to GLC without nanotubes. To test our assumption, we performed a series of molecular dynamics simulations during which we filled the GLC structure reinforced with (4,4) and (6,5) SWCNTs with potassium atoms at different mass fractions. The DOS distribution, Fermi energy, and quantum capacitance were calculated for each resulting potassium-functionalized GLC configuration.

## 2. Methods and Approaches

### 2.1. Building of Atomistic Models of GLC Reinforced with SWCNTs

The process of building an initial supercell of GLC was described in detail in our previous article [32]. This supercell contains 3891 atoms and has a volume  $V = 40.8 \cdot 41.8 \cdot 39.9 \text{ \AA}^3 = 68.05 \text{ nm}^3$ . The density of such a material was  $1.14 \text{ g/cm}^3$ , which agrees with known experimental data [33]. The mass fraction of fullerene-like elements in the supercell was 10.2%. Supercells of GLC with SWCNTs were constructed using the classical molecular dynamics method implemented in the LAMMPS software package (version 2021.4, Sandia National Laboratories, Albuquerque, NM, USA, Temple University, Philadelphia, PA, USA) [34]. Obtaining the equilibrium configuration of the structure was carried out in the following three stages: (1) static optimization using only the potential interaction between the nuclei—microcanonical NVE-ensemble of particles (at a constant number of particles, volume, and energy); (2) dynamic optimization using a thermostat—an isothermal NVT ensemble (at a constant number of particles, volume, and temperature); (3) dynamic optimization using a thermostat and barostat—isoenthalpic-isobaric NPT ensemble (at a constant number of particles, pressure, and temperature). In this case, holes were made in an initial supercell of GLC containing 3891 atoms, and thin SWCNTs were placed in them. A chiral nanotube (6,5) and an achiral nanotube (4,4) were taken as SWCNTs. Nanotubes of a larger diameter were not considered, because, with an increase in the diameter of the nanotubes, the number of atoms in the supercell also increases, which sharply increases the time of computer calculations. It is important that the selected nanotubes are characterized by different types of conductivity and topology. The simulation of the NVE ensemble was carried out until the maximum uncompensated force of interaction between the nuclei became equal to zero. The cutoff radii of the Coulomb and van der Waals interactions were equal to  $r_{\text{coulomb}} = r_{\text{vdw}} = 1 \text{ nm}$ . Next, a Nose–Hoover thermostat [35] was applied to the NVT ensemble, which made it possible to obtain an equilibrium structure at normal temperature  $T = 300 \text{ K}$ . The simulation was carried out with a time step of 0.5 fs for 50 ps.

To simulate the NPT ensemble, a Parinello–Raman barostat [36] with a reference pressure of  $P = 1$  bar was used. The simulation duration was 50 ps with a time step of 0.5 fs.

Thus, the following atomistic models of eight supercells of a 3D GLC nanomaterial reinforced with SWCNTs were constructed: four models with (6,5) nanotubes and four models with (4,4) nanotubes. The number of tubes in each model increased sequentially from one to four. Figure 1 shows GLC supercells with one and four (4,4) SWCNTs and GLC supercells with one and four (6,5) SWCNTs. Nanotubes (4,4) are highlighted in red, and nanotubes (6,5) are highlighted in blue. Each figure shows a supercell (periodic box) and a fragment of a 3D nanomaterial. It can be seen that the 3D nanomaterial of graphene/fullerene fragments is, as it were, reinforced with nanotubes.

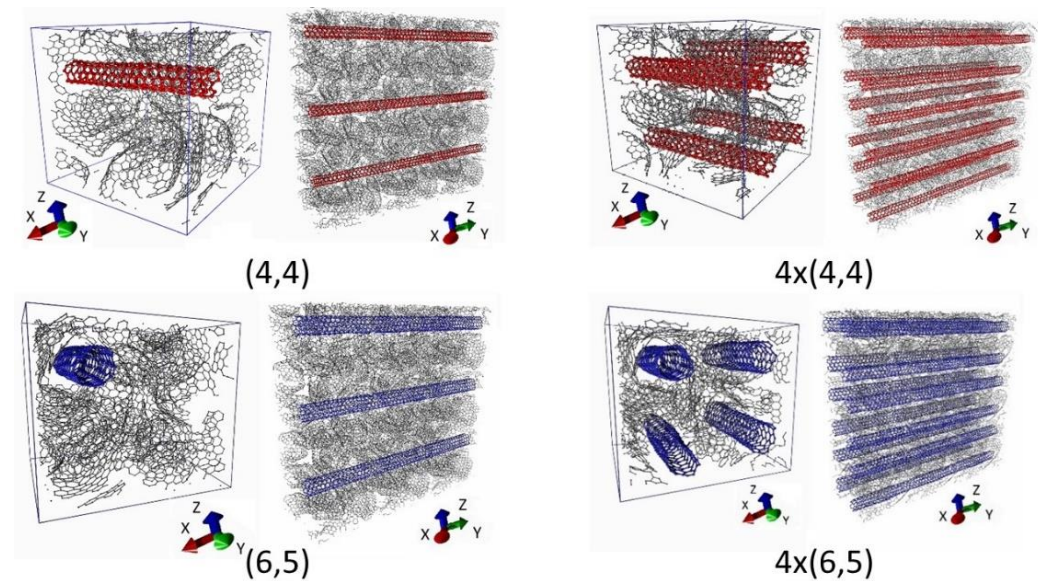


**Figure 1.** Atomistic models of a supercell (highlighted by a box) and a fragment of a 3D GLC reinforced with (4,4) and (6,5) SWCNTs.

For the constructed atomistic models with different mass fractions of nanotubes, the compressibility factor was calculated according to the following well-known formula [37]:

$$\langle \delta V^2 \rangle_{NPT} = V k_B T \eta \quad (1)$$

here  $\eta$  is the compressibility factor (the reciprocal of the volumetric compression factor),  $k_B$  is the Boltzmann constant. The compressibility factor was determined at the stage of modeling an isothermal–isobaric NPT ensemble of particles based on the analysis of volume fluctuations. The values of the compressibility factor and the bulk modulus for various models are presented in Table 1. As can be seen from Table 1, with an increase in the mass fraction of SWCNTs, an increase in the density of the material is observed in all cases under consideration. In this case, the chirality of the embedded SWCNT strongly affects the mechanical properties of the nanostructure under study. Thus, for models of a 3D nanomaterial with (6,5) nanotubes, which provide a higher density to the nanomaterial, the compressibility is lower compared to the nanomaterial based on (4,4) nanotubes. That is, with an increase in the SWCNT diameter, the mechanical responsiveness decreases, and the mechanical properties of the 3D nanomaterial begin to be determined by the mechanical properties of the SWCNTs themselves.

**Table 1.** Structural and elastic properties of GLC reinforced with (4,4) and (6,5) SWCNTs.

Number of Atoms in Supercell	% Mass Fraction of Nanotube, %	Density, g/cm <sup>3</sup>	Compressibility, GPa <sup>-1</sup>	Bulk Modulus, GPa
<b>GLC without SWCNTs</b>				
3891	0	1.18	0.519	1.93
<b>SWCNT (6,5)</b>				
4010	9.08	1.18	0.1091	9.17
4111	17.71	1.32	0.0793	12.61
4243	25.73	1.38	0.0539	18.55
4336	33.57	1.41	0.0519	19.27
<b>SWCNT (4,4)</b>				
3994	6.81	1.21	0.2071	4.83
4093	13.29	1.24	0.1072	9.35
4200	19.43	1.26	0.0788	12.69
4287	25.38	1.29	0.0682	14.71

Next, the resulting supercells of GLC reinforced with (4,4) and (6,5) SWCNTs were filled with potassium atoms at a potassium/carbon mass ratio ( $m(K):m(C)$ ) of 1:100 (0.01), 1:28.5 (0.035), 1:14 (0.07), 1:7.5 (0.13), 1:4.5 (0.23), and 1:3 (0.33) using the Nose–Hoover thermostat. After that, the atomic structure of supercells was reoptimized by means of molecular dynamics method using the reactive force field REAXFF [38]. The simulation was carried out with a time step of 0.5 fs for 50 ps at normal temperature  $T = 300$  K. Figure 2 demonstrates the optimized atomic structure of the supercells of GLC reinforced with (4,4) and (6,5) SWCNTs when filled with potassium at a potassium/carbon mass ratio of 1:100 and 1:14, respectively. This figure also shows a map of the local density distribution for these supercells. As can be seen, potassium fills predominantly the center region of GLC supercell. This corresponds to the interval of change in the coordinate  $X$  from 15 to 25 Å on the map of local density distribution. It should be noted that, at a potassium/carbon mass ratio of 1:14, the destruction of both graphene-like sheets and fullerene-like elements, and of (4,4) and (6,5) nanotubes is observed in the supercell of GLC-reinforced SWCNTs.

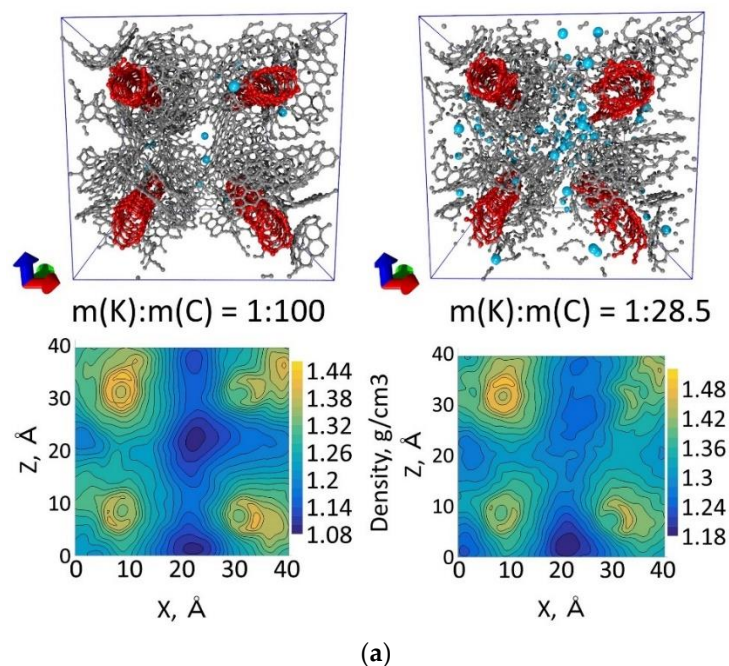


**Figure 2.** Cont.

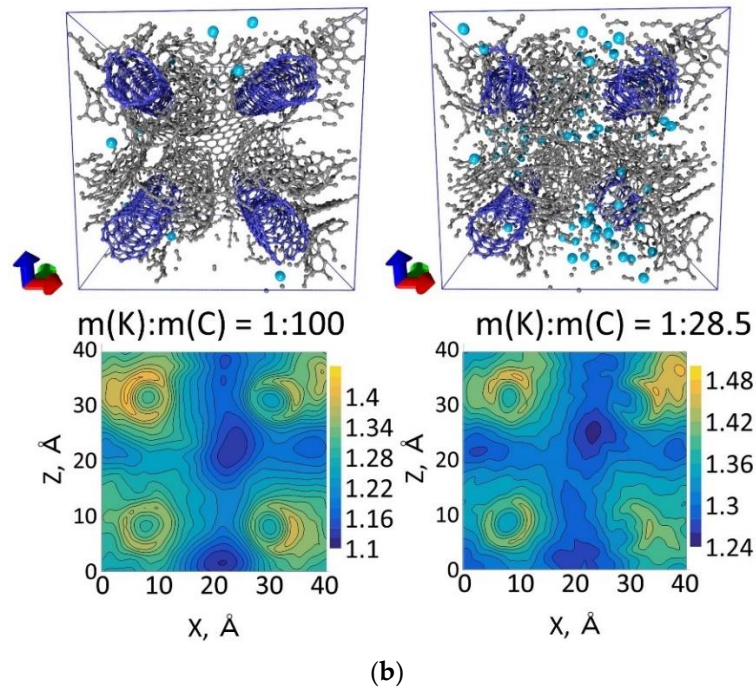


**Figure 2.** Supercells and maps of the local density distribution of GLC reinforced with (4,4) (a) and (6,5) SWCNTs (b) when filled with potassium at a mass ratio of potassium/carbon ( $m(K):m(C)$ ) of 1:100 and 1:14.

### 2.2. Calculation Details

To study the electronic properties of a 3D nanomaterial, the self-consistent-charge density-functional tight-binding (SCC-DFTB) method was used [39,40]. The total energy of the system in the framework of this approach is determined by the following expression:

$$E_{tot} = \sum_{i\mu\nu} c_{\mu}^i c_{\nu}^i H_{\mu\nu}^0 + \frac{1}{2} \sum_{\alpha\beta} \gamma_{\alpha\beta} \Delta q_{\alpha} \Delta q_{\beta} + E_{rep} + E_{dis}, \quad (2)$$

where  $c_{\mu}^i$  and  $c_{\nu}^i$  are weight coefficients in the expansion into atomic orbitals,  $\Delta q_{\alpha}$  and  $\Delta q_{\beta}$  are charge fluctuations on atoms  $\alpha$  and  $\beta$ , respectively,  $\gamma_{\alpha\beta}$  is a function that decreases exponentially with increasing distance between atoms  $\alpha$  and  $\beta$ ,  $E_{rep}$  is term describing the repulsive interaction at small distances;  $E_{dis}$  is the van der Waals interaction energy. The van der Waals interaction was modeled using the universal force field (UFF), which supports the description of the interaction of various atoms [41]. The full sp-basis for carbon atoms and the s-basis for potassium atoms were used. All calculations were carried out at the  $\Gamma$  point. The SCC-DFTB calculations were performed using the DFTB+ software package version 20.2 (University of Bremen, Bremen, Germany) [42].

The calculation of the quantum capacity was carried out in accordance with the formula of the following form [43]:

$$C_q(U) = \frac{1}{mU} \int_0^U eD(E_F - eU')dU', \quad (3)$$

where  $m$  is the mass of the object,  $U$  is the displacement calculated as a change in the Fermi energy with a change in the charge of the object,  $e$  is the elementary charge,  $D$  is the DOS function for the applied displacement, and  $E_F$  is the Fermi energy.

### 3. Results and Discussion

We have studied how the electronic properties of GLC reinforced with (4,4) and (6,5) nanotubes will change at different potassium/carbon mass ratios. Figure 3 shows the plots of changes in the Fermi energy for the GLC structures reinforced SWCNTs when filled

with potassium. For most structures, at a mass ratio of potassium to carbon of 1:100 (0.01), an increase in the Fermi energy is observed, since the pores of the GLC are filled with potassium without destroying the carbon hexagonal cells, as shown in Figure 2a,b (picture on the left). However, an increase in the number of potassium atoms (a potassium/carbon mass ratio of more than 1:28.5 (0.035)) leads to the destruction of the GLC atomic structure with nanotubes (Figure 2a,b, picture on the right). This process is accompanied by a shift of the Fermi level along the energy axis to the left relative to zero eV and, accordingly, an increase in the work function electron from the material. At a potassium/carbon mass ratio of more than 1:7.5 (0.13), a significant number of hexagonal elements of graphene-like sheets have already been destroyed, and only islands of local density maxima of fullerene-like and nanotube carbon elements remain, which do not undergo further destruction. Thus, the subsequent decrease in the work function occurs due to the shift of the Fermi level along the energy axis to the right relative to 0 eV upon the addition of potassium atoms. The maximum decrease in the work function by  $\sim 0.3$  eV was achieved at a mass ratio of potassium/carbon of 1:4.5 (0.23) for the SWCNT (6,5).

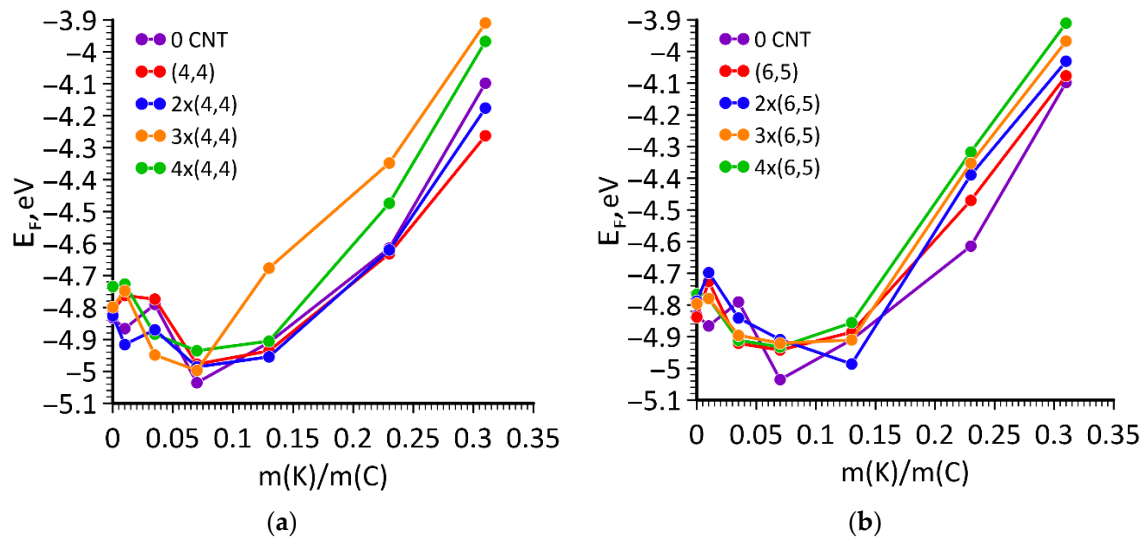


**Figure 3.** Dependence of the Fermi energy  $E_F$  on the potassium/carbon mass ratio ( $m(K)/m(C)$ ) for GLC reinforced (4,4) (a) and (6,5) (b) SWCNTs.

It can be noted that, apart from the  $3 \times (4,4)$  case, the highest Fermi energy is observed for structures with four nanotubes, i.e., the  $4 \times (4,4)$  and  $4 \times (6,5)$  configurations, which have greater elasticity than structures with less than the number of nanotubes according to the data in Table 1. The diameter of the nanotubes also affects the Fermi level when filled with potassium. The Fermi energy in almost all cases is greater for GLCs with (6,5) SWCNTs.

Figure 4 shows the distributions of DOS of GLC reinforced with (4,4) and (6,5) SWCNTs. For the convenience of analyzing the obtained distributions, the Fermi level on the plots is shifted to zero eV. It can be seen that when the GLC structure with SWCNTs is filled with potassium, the number of available electronic states at the Fermi level increases, which significantly improves the emission properties of the material and, as will be shown below, the capacitive properties of the material. Thus, at a potassium/carbon mass ratio of 1:100 (0.01), the DOS maximum ( $853.43 \text{ eV}^{-1}$ ) for GLC reinforced with two (4,4) SWCNTs increases by 3.6%, and the DOS maximum ( $943.96 \text{ eV}^{-1}$ ) for GLC-reinforced four (6,5) SWCNTs increases by 12.8% as compared to the DOS maximum ( $822.74 \text{ eV}^{-1}$ ) of GLC without nanotubes.

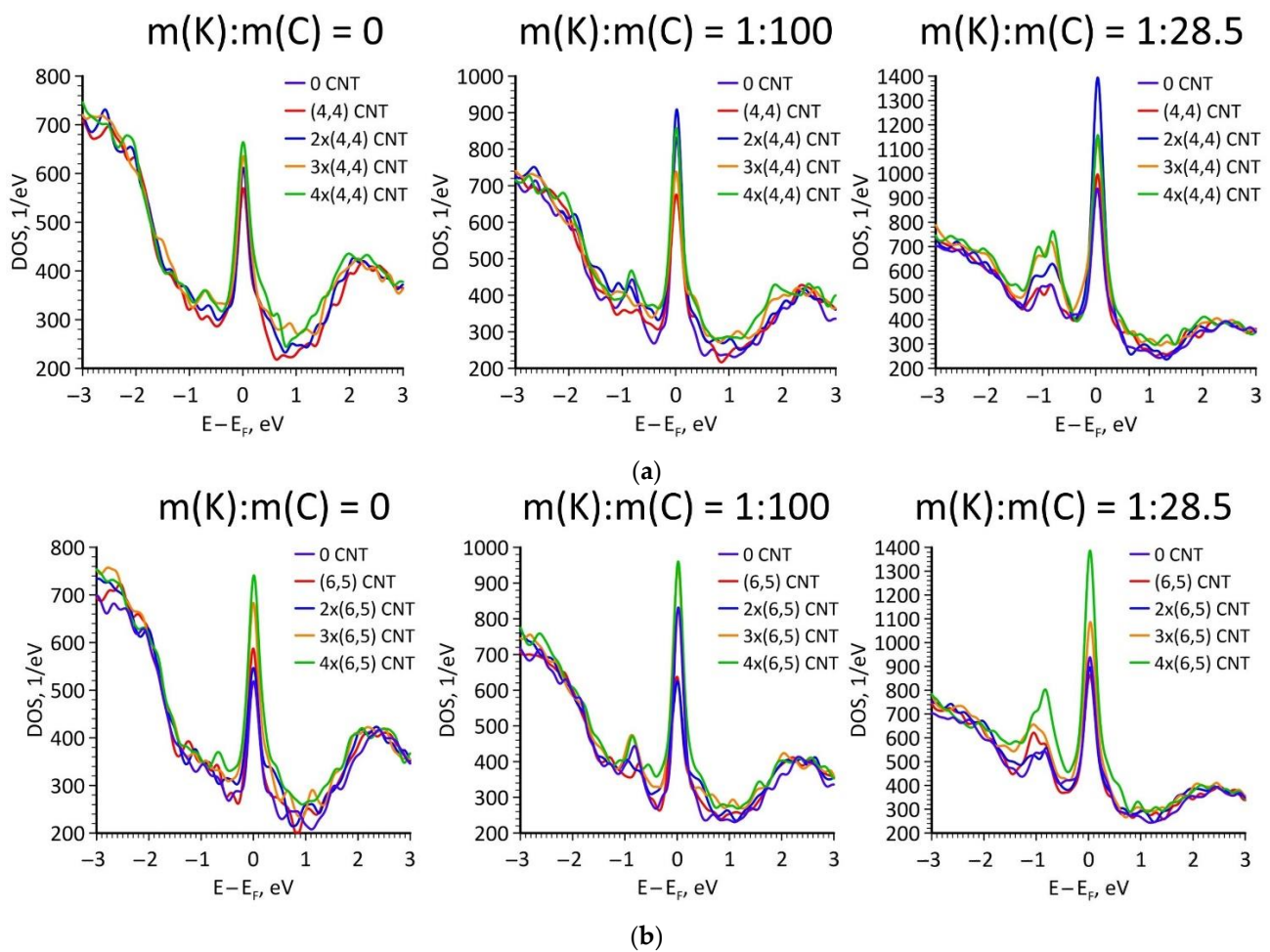


**Figure 4.** DOS of GLC reinforced with (4,4) SWCNTs (a) at potassium content 0, 1:100, and 1:28.5, and with (6,5) SWCNTs (b) at potassium content 0, 1:100, and 1:28.5.

The effect of potassium on the electronic properties of GLC reinforced with nanotubes was also estimated from the quantum capacitance. The results of calculating the quantum capacitance are shown in Figure 5. It can be seen from the figure that the calculated quantum capacitance profiles largely repeat the DOS profiles. Thus, when filling with potassium at zero voltage (actually at the Fermi level), the quantum capacitance almost doubles at a potassium/carbon mass ratio of 1:28.5 (0.035).

The influence of the nanotube diameter on the quantum capacitance is also noticeable. For GLC with (4,4) SWCNTs, with an increase in potassium atoms, the highest quantum capacity is observed when GLC is reinforced with two tubes. While in the case of reinforcement with (6,5) SWCNTs, the maximum quantum capacitance is observed for the atomic configuration of GLC with four nanotubes, as in the case of the DOS distribution. The obtained results significantly exceed the quantum capacitance of other composite carbon nanomaterials, in particular, graphene–nanotube films with an island structure subjected to axial tensile deformation [43] and pillared graphene films [44]. For example, the maximum quantum capacitance of graphene–nanotube film was 1197 F/g at an axial stretch of 5% [43]. The pillared graphene film modified with boron (B) clusters had a maximum quantum capacitance of ~1266 F/g in the case of five B12 clusters [44]. The quantum capacitance of GLC reinforced with SWCNTs also exceeds the ones of some other materials. In particular, the maximum quantum capacitance of the boron-doped (6, 6) CNTs in negative and positive voltages was 304 F/g and 760 F/g, respectively. For boron-doped (16, 16) CNTs, these values were found to be 335 F/g and 659 F/g, respectively [45]. The quantum capacitance of the MnSe<sub>2</sub>/CNT composite does not exceed 1300 F/g [46].

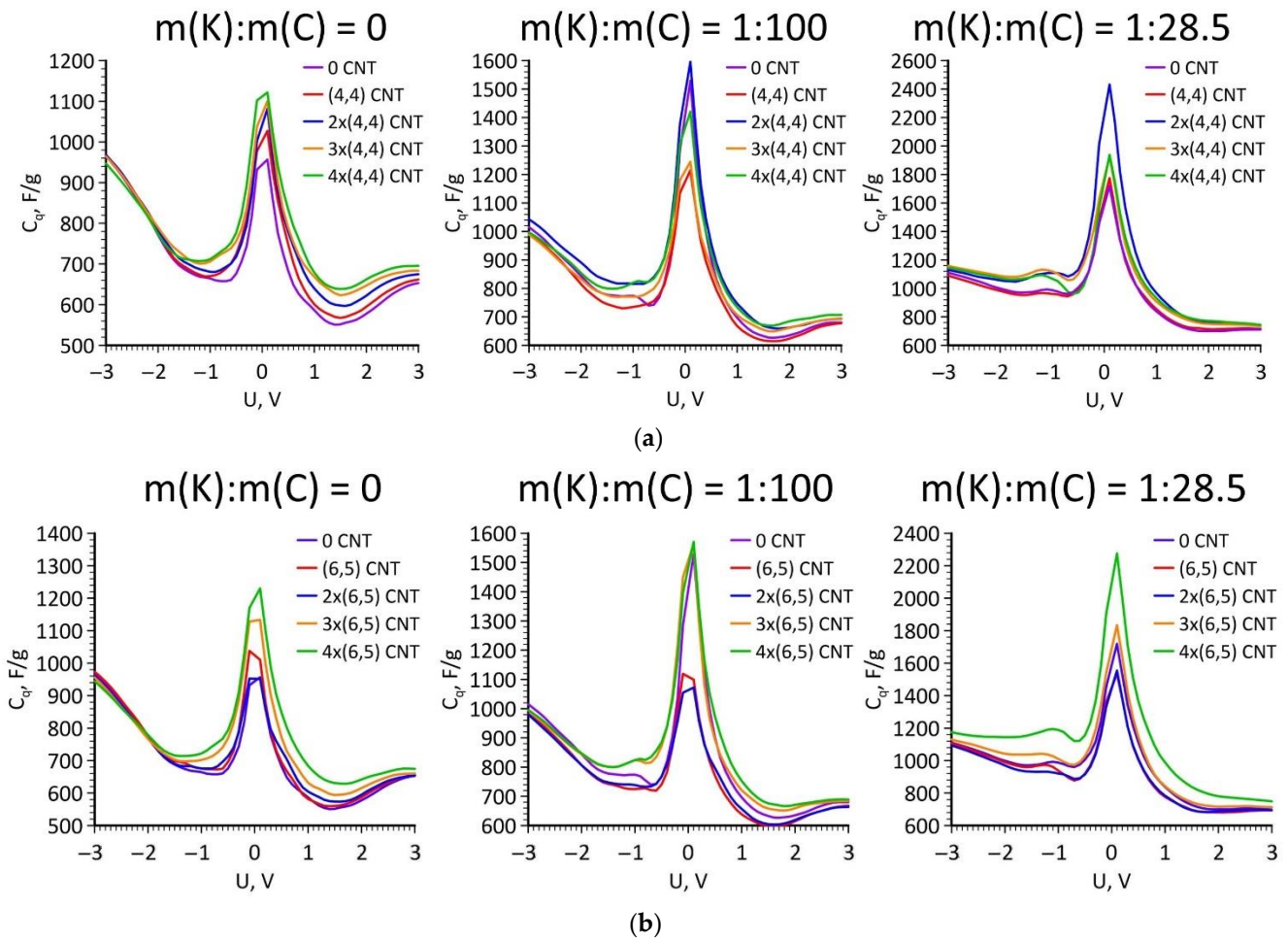


**Figure 5.** Quantum capacitance of GLC reinforced with (4,4) SWCNTs (a) at potassium content 0, 1:100, and 1:28.5, and with (6,5) SWCNTs (b) at potassium content 0, 1:100, and 1:28.5.

#### 4. Conclusions

Thus, using the molecular dynamics method, atomistic models of supercells of a new composite GLC nanomaterial with an island-type topology due to the presence of reinforcing SWCNTs of subnanometer diameter in the graphene/fullerene fragments were constructed. It has been established that the bulk modulus of GLC at the maximum mass fraction of nanotubes increases by 7–10 times, depending on the nanotube diameter, as compared to the GLC without SWCNTs. Nanotubes of larger diameter also provide greater elasticity to the composite. Based on the results of SCC-DFTB calculations, regularities in the change in the electrophysical parameters of GLC reinforced with (4,4) and (6,5) SWCNTs when filled with potassium were revealed. We have shown that, at a potassium/carbon mass ratio of 1:100 (0.01), the maximum DOS of GLC reinforced with (4,4) and (6,5) SWCNTs increases by 3.6% and 12.8%, respectively, as compared to the maximum DOS of GLC without nanotubes. At a potassium/carbon mass ratio of 1:4.5 (0.23), the maximum decrease in the work function for the GLC reinforced with (4,4) SWCNTs was ~0.2 eV, and for the GLC reinforced with (6,5) SWCNTs was ~0.3 eV. The presence of nanotubes in the GLC structure also contributes to an increase in the quantum capacitance of the carbon nanomaterial. The quantum capacitance of GLC reinforced with four (4,4) and (6,5) SWCNTs already at a mass ratio of potassium/carbon of 1:28.5 increases by ~9.4% (1752.63 F/g) and 24.1% (2092.04 F/g), respectively, as compared to the nanotubeless GLC (1587.93 F/g). Based on the simulation results obtained, it can be concluded that the potassium-functionalized SWCNT-reinforced GLC nanomaterial is promising for use in modern nanoelectronic devices, including emission devices.

**Author Contributions:** Conceptualization, O.E.G.; methodology, O.E.G.; funding acquisition, M.M.S. and O.E.G.; investigation, O.E.G., A.A.P. and M.M.S.; writing—original draft preparation, A.A.P.; writing—review and editing, M.M.S. and O.E.G.; supervision, O.E.G. All authors have read and agreed to the published version of the manuscript.

**Funding:** The building of atomistic models of GLC reinforced with nanotubes was funded by the Council on grants of the President of the Russian Federation (project No. MK-2289.2021.1.2). The research of electronic properties and quantum capacitance of GLC was funded by Ministry of Science and Higher Education of Russian Federation in the frame work of the government task (project No. FSRR-2020-0004).

**Institutional Review Board Statement:** Not applicable.

**Informed Consent Statement:** Not applicable.

**Data Availability Statement:** Not applicable.

**Conflicts of Interest:** The authors declare no conflict of interest.

## References

1. Sharma, S. Glassy Carbon: A Promising Material for Micro and Nanomanufacturing. *Materials* **2018**, *11*, 1857. [[CrossRef](#)] [[PubMed](#)]
2. Jurkiewicz, K.; Pawlyta, M.; Zygadło, D.; Chrobak, D.; Duber, S.; Wrzalik, R.; Ratuszna, A.; Burian, A. Evolution of glassy carbon under heat treatment: Correlation structure–mechanical properties. *J. Mat. Sci.* **2018**, *53*, 3509–3523. [[CrossRef](#)]
3. Bauer, J.; Schroer, A.; Schwaiger, R.; Kraft, O. Approaching theoretical strength in glassy carbon nanolattices. *Nat. Mater.* **2016**, *15*, 438–443. [[CrossRef](#)]
4. Slepchenkov, M.M.; Shmygin, D.S.; Zhang, G.; Glukhova, O.E. Controlling the electronic properties of 2D/3D pillared graphene and glass-like carbon via metal atom doping. *Nanoscale* **2019**, *11*, 16414–16427. [[CrossRef](#)] [[PubMed](#)]
5. Jurkiewicz, K.; Duber, S.; Fischer, H.E.; Burian, A. Modelling of glass-like carbon structure and its experimental verification by neutron and X-ray diffraction. *J. Appl. Cryst.* **2017**, *50*, 36–48. [[CrossRef](#)]
6. Zampardi, G.; La Mantia, F.; Schuhmann, W. Determination of the formation and range of stability of the SEI on glassy carbon by local electrochemistry. *RSC Adv.* **2015**, *5*, 31166–31171. [[CrossRef](#)]
7. Shimizu, A.; Tachikawa, H. Molecular dynamics simulation on diffusion of lithium atom pair in C150H30 cluster model for glassy carbon at very low temperatures. *Electrochim. Acta* **2003**, *48*, 1727–1733. [[CrossRef](#)]
8. Sharma, S.; Kamath, R.; Madou, M. Porous glassy carbon formed by rapid pyrolysis of phenol-formaldehyde resins and its performance as electrode material for electrochemical double layer capacitors. *J. Anal. Appl. Pyrolysis* **2014**, *108*, 12–18. [[CrossRef](#)]
9. Bozym, D.J.; Uralcan, B.; Limmer, D.T.; Pope, M.A.; Szamreta, N.J.; Debenedetti, P.G.; Aksay, I.A. Anomalous Capacitance Maximum of the Glassy Carbon–Ionic Liquid Interface through Dilution with Organic Solvents. *J. Phys. Chem. Lett.* **2015**, *6*, 2644–2648. [[CrossRef](#)]
10. Palanisamy, S.; Ku, S.; Chen, S.-M. Dopamine sensor based on a glassy carbon electrode modified with a reduced graphene oxide and palladium nanoparticles composite. *Microchim. Acta* **2013**, *180*, 1037–1042. [[CrossRef](#)]
11. Cui, F.; Zhang, X. Electrochemical sensor for epinephrine based on a glassy carbon electrode modified with graphene/gold nanocomposites. *J. Elec. Chem.* **2012**, *669*, 35–41. [[CrossRef](#)]
12. Tajik, S.; Beitollahi, H. A Sensitive Chlorpromazine Voltammetric Sensor Based on Graphene Oxide Modified Glassy Carbon Electrode. *Anal. Bioanal. Chem. Res.* **2019**, *6*, 171–182.
13. Tajik, S.; Beitollahi, H.; Biparva, P. Methyl dopa electrochemical sensor based on a glassy carbon electrode modified with Cu/TiO<sub>2</sub> nanocomposite. *J. Serbian Chem. Soc.* **2018**, *83*, 863–874. [[CrossRef](#)]
14. Devi, M.; Vomero, M.; Fuhrer, E.; Castagnola, E.; Gueli, C.; Nimbalkar, S.; Hirabayashi, M.; Kassegne, S.; Stieglitz, T.; Sharma, S. Carbon-based neural electrodes: Promises and challenges. *J. Neural. Eng.* **2021**, *18*, 041007. [[CrossRef](#)] [[PubMed](#)]
15. Uskoković, V. A historical review of glassy carbon: Synthesis, structure, properties and applications. *Carbon Trends* **2021**, *5*, 100116. [[CrossRef](#)]
16. Jovanovic, Z.; Kalijadis, A.; Vasiljevic-Radovic, D.; Eric, M.; Lausevic, M.; Mentus, S.; Lausevic, Z. Modification of glassy carbon properties under low energy proton irradiation. *Carbon* **2011**, *49*, 3737–3746. [[CrossRef](#)]
17. Serp, P.; Machado, B. *Nanostructured Carbon Materials for Catalysis*, 1st ed.; Royal Society of Chemistry: London, UK, 2015; pp. 1–45.
18. Arkhipov, A.; Davydov, S.; Gabdullin, P.; Gnuchev, N.; Kravchik, A.; Krel, S. Field-induced electron emission from nanoporous carbons. *J. Nanomater.* **2014**, *2014*, 190232. [[CrossRef](#)]
19. Kravchik, A.E.; Kukushkina, J.A.; Sokolov, V.V.; Tereshchenko, G.F. Structure of nanoporous carbon produced from boron carbide. *Carbon* **2006**, *44*, 3263–3268. [[CrossRef](#)]
20. Pykal, M.; Jurečka, P.; Karlický, F.; Otyepka, M. Modelling of graphene functionalization. *Phys. Chem. Chem. Phys.* **2016**, *18*, 6351–6372. [[CrossRef](#)]

21. Harris, P.J.F. Fullerene-Related Structure of Commercial Glassy Carbons. *Philos. Mag.* **2004**, *84*, 3159–3167. [[CrossRef](#)]
22. Harris, P.J.F.; Tsang, S.C. High-Resolution Electron Microscopy Studies of Non-Graphitizing Carbons. *Philos. Mag. A* **1997**, *76*, 667–677. [[CrossRef](#)]
23. Harris, P.J.F. Fullerene-Like Models for Microporous Carbon. *J. Mater. Sci.* **2013**, *48*, 565–577. [[CrossRef](#)]
24. Sharma, S.; Kumar, C.N.S.; Korvink, J.G.; Kübel, C. Evolution of Glassy Carbon Microstructure: In Situ Transmission Electron Microscopy of the Pyrolysis. *Process. Sci. Rep.* **2018**, *8*, 16282. [[CrossRef](#)]
25. Carpenter, A.C.; Hunt, C.E. High-current, low-cost field emission triode using a reticulated vitreous carbon cathode. *J. Vac. Sci. Technol. B* **2010**, *28*, C2C37–C2C40. [[CrossRef](#)]
26. Gay, S.; Orlanducci, S.; Passeri, D.; Rossic, M.; Terranova, M.L. Nanoshaping field emitters from glassy carbon sheets: A new functionality induced by H-plasma etching. *Phys. Chem. Chem. Phys.* **2016**, *18*, 25364–25372. [[CrossRef](#)]
27. Smith, B.C.; Hunt, C.E.; Brodiec, I.; Carpenter, A.C. High-performance field-emission electron gun using a reticulated vitreous carbon cathode. *J. Vac. Sci. Technol. B* **2011**, *29*, 02B108. [[CrossRef](#)]
28. Egorov, N.; Sheshin, E. Carbon-Based Field-Emission Cathodes. In *Field Emission Electronics*, 1st ed.; Springer: Berlin/Heidelberg, Germany, 2017; Volume 60, pp. 295–367.
29. Figueiredo, J.L. Functionalization of porous carbons for catalytic applications. *J. Mater. Chem. A* **2013**, *1*, 9351–9364. [[CrossRef](#)]
30. Long, C.; Jiang, L.; Wu, X.; Jiang, Y.; Yang, D.; Wang, C.; Wei, T.; Fan, Z. Facile synthesis of functionalized porous carbon with three-dimensional interconnected pore structure for high volumetric performance supercapacitors. *Carbon* **2015**, *93*, 412–420. [[CrossRef](#)]
31. Benzigar, M.R.; Talapaneni, S.N.; Joseph, S.; Ramadass, K.; Singh, G.; Scaranto, J.; Ravon, U.; Al-Bahily, K.; Vinu, A. Recent advances in functionalized micro and mesoporous carbon materials: Synthesis and applications. *Chem. Soc. Rev.* **2018**, *47*, 2680–2721. [[CrossRef](#)]
32. Glukhova, O.E.; Slepchenkov, M.M. Electronic Properties of the Functionalized Porous Glass-Like Carbon. *J. Phys. Chem. C* **2016**, *120*, 17753–17758. [[CrossRef](#)]
33. Zhao, Z.; Wang, E.F.; Yan, H.; Kono, Y.; Wen, B.; Bai, L.; Shi, F.; Zhang, J.; Kenney-Benson, C.; Park, C.; et al. Nanoarchitected Materials Composed of Fullerene-Like Spheroids and Disordered Graphene Layers With Tunable Mechanical Properties. *Nat. Commun.* **2015**, *6*, 6212. [[CrossRef](#)] [[PubMed](#)]
34. LAMMPS Molecular Dynamics Simulator. Available online: <https://www.lammps.org/> (accessed on 15 January 2021).
35. Nose, S. A molecular dynamics method for simulations in the canonical ensemble. *Mol. Phys.* **1984**, *52*, 255–268. [[CrossRef](#)]
36. Parrinello, M.; Rahman, A. Polymorphic transitions in single crystals: A new molecular dynamics method. *J. Appl. Phys.* **1981**, *52*, 7182–7190. [[CrossRef](#)]
37. Allen, M.P.; Tildesley, D.J. *Computer Simulation of Liquids*, 2nd ed.; Oxford University Press: Oxford, UK, 2017; pp. 95–147.
38. Senftle, T.P.; Hong, S.; Islam, M.M.; Kylasa, S.B.; Zheng, Y.; Shin, Y.K.; Junkermeier, C.; Engel-Herbert, R.; Janik, M.J.; Aktulga, H.M.; et al. The ReaxFF Reactive Force-Field: Development, Applications and Future Directions. *Comput. Mater.* **2016**, *2*, 15011–15025. [[CrossRef](#)]
39. Elstner, M.; Porezag, D.; Jungnickel, G.; Elsner, J.; Haugk, M.; Frauenheim, T.; Suhai, S.; Seifert, G. Self-Consistent-Charge Density-Functional Tight-Binding Method for Simulations of Complex Materials Properties. *Phys. Rev. B* **1998**, *58*, 7260–7268. [[CrossRef](#)]
40. Elstner, M.; Seifert, G. Density Functional Tight Binding. *Phil. Trans. R. Soc.* **2014**, *372*, 20120483. [[CrossRef](#)]
41. Rappe, A.K.; Casewit, C.J.; Colwell, K.S.; Goddard, W.A.; Skiff, W.M. UFF, a Full Periodic Table Force Field for Molecular Mechanics and Molecular Dynamics Simulations. *J. Am. Chem. Soc.* **1992**, *114*, 10024–10035. [[CrossRef](#)]
42. Hourahine, B.; Aradi, B.; Blum, V.; Bonafé, F.; Buccheri, A.; Camacho, C.; Cevallos, C.; Deshayé, M.Y.; Dumitrică, T.; Dominguez, A.; et al. DFTB+, a Software Package for Efficient Approximate Density Functional Theory Based Atomistic Simulations. *J. Chem. Phys.* **2020**, *152*, 124101. [[CrossRef](#)]
43. Slepchenkov, M.M.; Barkov, P.V.; Glukhova, O.E. In Silico Study of the Electrically Conductive and Electrochemical Properties of Hybrid Films Formed by Bilayer Graphene and Single-Wall Nanotubes under Axial Stretching. *Membranes* **2021**, *11*, 658. [[CrossRef](#)]
44. Kolosov, D.A.; Glukhova, O.E. Boron-Decorated Pillared Graphene as the Basic Element for Supercapacitors: An Ab Initio Study. *Appl. Sci.* **2021**, *11*, 3496. [[CrossRef](#)]
45. Mousavi-Khoshdel, S.M.; Jahanbakhsh-bonab, P.; Targholi, E. Structural, electronic properties, and quantum capacitance of B, N and P-doped armchair carbon nanotubes. *Phys. Lett. A* **2016**, *380*, 3378–3383. [[CrossRef](#)]
46. Samal, R.; Bhat, M.; Kapse, S.; Thapa, R.; Late, D.J.; Rout, C.S. Enhanced energy storage performance and theoretical studies of 3D cuboidal manganese diselenides embedded with multiwalled carbon nanotubes. *J. Colloid Interface Sci.* **2021**, *598*, 500–510. [[CrossRef](#)] [[PubMed](#)]